Published in final edited form as:
Bone. 2011 August ; 49(2): 250–256. doi:10.1016/j.bone.2011.03.770.

Dose response of bone-targeted enzyme replacement for murine hypophosphatasia

Manisha C. Yadav[1], **Isabelle Lemire**[2], **Pierre Leonard**[2], **Guy Boileau**[3], **Laurent Blond**[3], **Martin Beliveau**[4], **Esther Cory**[5], **Robert L. Sah**[5], **Michael P. Whyte**[6], **Philippe Crine**[2], and **José Luis Millán**[1]

[1]Sanford Children's Health Research Center, Sanford-Burnham Medical Research Institute, La Jolla, CA 92037, USA

[2]Enobia Pharma, Inc., Montréal, QC, Canada

[3]University of Montréal, Montréal, QC, Canada

[4]Pharsight, Montreal, QC, Canada

[5]Department of Bioengineering, University of California,-San Diego, La Jolla, CA 92037, USA

[6]Shriners Hospital for Children and Washington University, St. Louis, MO, 63131 and 63110, USA

Abstract

Hypophosphatasia (HPP) features rickets or osteomalacia from tissue-nonspecific alkaline phosphatase (TNSALP) deficiency due to deactivating mutations within the *ALPL* gene. Enzyme replacement therapy with a bone-targeted, recombinant TNSALP (sALP-FcD_{10}, renamed ENB-0040) prevents manifestations of HPP when initiated at birth in TNSALP knockout (*Akp2*$^{-/-}$) mice. Here, we evaluated the dose-response relationship of ENB-0040 to various phenotypic traits of *Akp2*$^{-/-}$ mice receiving daily subcutaneous (SC) injections of ENB-0040 from birth at 0.5, 2.0, or 8.2 mg/kg for 43 days. Radiographs, μCT, and histomorphometric analyses documented better bone mineralization with increasing doses of ENB-0040. We found a clear, positive correlation between ENB-0040 dose and prevention of mineralization defects of the feet, rib cage, lower limbs, and jaw bones. According to a dose-response model, the ED_{80} (the dose prevents the bone defects in 80% of mice) was 3.2, 2.8 and 2.9 mg/kg/day for these sites, respectively. Long bones seemed to respond to lower daily doses of ENB-0040. There was also a positive relationship between ENB-0040 dose and survival. Median survival, body weight, and bone length all improved with increasing doses of ENB-0040. Urinary PP_i concentrations remained elevated in all treatment groups, indicating that while this parameter is a good biochemical marker for diagnosing HPP, it may not be a good follow up marker for evaluating response to treatment when administering bone-targeted TNSALP. These dose-response relationships strongly support the pharmacological efficacy of ENB-0040 for HPP, and provide the experimental basis for the therapeutic range of ENB-0040 chosen for clinical trials.

Address for correspondence: Professor José Luis Millán, PhD, Sanford Children's Health Research Center, Sanford-Burnham Medical Research Institute, 10901 North Torrey Pines Road, La Jolla, CA 92037, Tel: (858) 646-3130; Fax: (858) 646-3195, millan@sanfordburnham.org.

Keywords

alkaline phosphatase; calcification; ENB-0040; rickets; osteomalacia

Introduction

Hypophosphatasia (HPP) is the inborn-error-of-metabolism characterized by subnormal alkaline phosphatase (ALP) activity in serum and features rickets or osteomalacia [1-3] due to loss-of-function mutation within the tissue-nonspecific alkaline phosphatase (TNSALP) gene (*ALPL*) [4-6]. The clinical severity of HPP ranges widely and spans complete absence of bone mineralization and stillbirth, to spontaneous fractures and loss of teeth in adult life [2,3]. According to a traditional clinical nosology, the most severe to the mildest forms are perinatal, infantile, childhood, adult, and odontohypophosphatasia [3, 7].

TNSALP null mice (*Akp2*$^{-/-}$) phenocopy infantile HPP extremely well [8, 9]. They are born with a normally mineralized skeleton, but develop rickets at about 6 days of age and die between day 16-20 suffering severe skeletal hypomineralization, episodes of apnea, and seizures [8-12]. The primary biochemical defect, TNSALP isozyme deficiency, leads to extracellular accumulation of its natural substrates including pyridoxal-5′-phosphate (PLP), the principal circulating form of vitamin B6, and inorganic pyrophosphate (PP_i), a potent inhibitor of mineralization [13]. Impaired hydrolysis of PLP causes intracellular deficiency of vitamin B6 in the central nervous system and thereby reduced brain levels of gamma-aminobutyric acid and seizures [10, 12]. This abnormality is evident not only in *Akp2*$^{-/-}$ mice [8-10], but also sometimes in severely affected infants [11]. Rickets and osteomalacia in HPP are due to the accumulation in cartilage or bone matrix of extracellular PP_i, caused by reduced pyrophosphatase activity of TNSALP [2, 3, 14-18].

To-date, there is no established medical treatment for HPP [2, 3]. Attempted enzyme replacement therapy (EzRT) using intravenous (IV) infusions of ALP-rich plasma from Paget bone disease patients, purified human liver ALP, or purified human placental ALP was followed by failure to rescue severely affected infants [19-22]. However, in 2008, we reported that newborn *Akp2*$^{-/-}$ mice receiving a daily, high-dose (8.2 mg/kg), subcutaneous (SC) injection of a bone-targeted form of recombinant TNSALP, sALP-FcD_{10} (renamed ENB-0040), grew normally and appeared well without skeletal or dental disease, or epilepsy, demonstrating that this EzRT could prevent all of the manifestations of infantile HPP in this murine model [23; 24].

Here, we present a dose-response study that establishes the optimal dose of ENB-0040 for prevention of HPP in *Akp2*$^{-/-}$ mice, and thereby enhances the preclinical foundation for EzRT trials for HPP patients.

Materials and methods

Mouse model of Infantile HPP

The *Akp2*$^{-/-}$ knockout mice, created by insertion of the Neo cassette into exon 6 of the mouse TNSALP gene (*Akp2*) via homologous recombination, functionally inactivates the *Akp2* gene resulting in no detectable TNSALP mRNA or protein [8]. These *Akp2*$^{-/-}$ mice, maintained in a 12.5% C57Bl/6 - 87.5% 129J background, closely phenocopy infantile HPP [8, 9]. Like those severely affected patients, *Akp2*$^{-/-}$ mice have global deficiency of TNSALP activity, extracellular accumulation of the ALP substrates PP_i, PLP, and phosphoethanolamine (PEA), and postnatally manifest an acquired defect in mineralization of skeletal matrix leading to radiographically and histologically obvious rickets [9]. They

have stunted growth and also develop seizures and apnea, and die between postnatal days 10-12 [8-10]. Pyridoxine supplementation briefly suppresses their seizures and extends their lifespan, but only until postnatal days 18-22 [10, 12]. Therefore, all animals (breeders, nursing mothers and their pups, and weanlings) in this study were given free access to modified laboratory rodent diet 5001 containing increased levels (325 ppm) of pyridoxine. The *Akp2*$^{-/-}$ homozygous mice were identified at birth (Day 0) by PCR of tissue biopsies using specific primers to exon 6 of the mouse TNSALP gene: 5′-GTCCGTGGGCATTGTGACTACCAC-3′ and 5′-TGCTGCTCCACTCACGTCG-3′.

Bone-targeted, recombinant, human TNSALP

The ENB-0040 (sALP-FcD_{10}) fusion protein contains recombinant human soluble TNSALP (sALP), the constant region of human IgG_1 Fc domain (Fc) to facilitate purification, and a deca-aspartate motif (D_{10}) for bone mineral targeting [24]. The expression, purification, and characterization of this fusion protein have been published [23]. Lot number PUR012F01 of ENB-0040 [produced under Current Good Manufacturing Practices (cGMP) formulated at 0.15, 0.6 and 2.5 mg/mL in 25 mmol/L sodium phosphate, 150 mmol/L sodium chloride, pH 7.4] was used in the current study.

Dose-response study

Akp2$^{-/-}$ mice were divided into 5 groups: Group 1 (Vehicle): *Akp2*$^{-/-}$ mice treated with vehicle SC daily (n=21); Group 2 (Tx-0.5): *Akp2*$^{-/-}$ mice treated with ENB-0040 at 0.5 mg/kg SC daily (n=18); Group 3 (Tx-2.0): *Akp2*$^{-/-}$ mice treated with ENB-0040 at 2.0 mg/kg SC daily (n=20); and Group 4 (Tx-8.2): *Akp2*$^{-/-}$ mice treated with ENB-0040 at 8.2 mg/kg SC daily (n=19). Group 5 (WT): wild-type littermates of *Akp2*$^{-/-}$ mice served as reference animals and did not receive injections (n=33). Injections were administered between 8:00 and 11:00 AM, and dose volume was set at 3.3 mL/kg body weight. The actual volume given was calculated and adjusted based on the daily body weight measured prior to injection. Vehicle or ENB-0040 was injected SC into the scapular region. All treatments began on postnatal Day 1, and were repeated daily for up to 43 days or until the time of necropsy.

Terminal procedures

Necropsy was performed on Day 44, 24 hours after the final injection of ENB-0040 for those animals that completed the experimental protocol, or sooner for those animals that appeared terminally ill. All animals were euthanized by bilateral thoracotomy under isoflurane anesthesia. The necropsy consisted of a gross pathology check, with a piece of ear collected to confirm the *Akp2*$^{-/-}$ genotype. The bone samples were cleaned, fixed in 10% neutral buffered formalin for 3 days at 2 to 8°C, and then transferred to 70% ethanol for storage at 2 to 8°C. Femur and tibia lengths were measured using a caliper.

Radiographic analysis

Radiographic images were obtained with a Faxitron MX-20 DC4 (Faxitron X-ray Corporation, Wheeling, IL), using energy of 26 kV and an exposure time of 10 seconds. Defects in bone mineralization were classified in a blinded fashion by a veterinarian radiologist. Animals were “Abnormal” if at least one bone structure (including secondary ossification centers) was absent.

Histological analyses

The femora and tibiae of treated and untreated mice were fixed in 10% formalin. Sections were prepared according to the Kawamoto method [25] with slight modifications. Briefly, the specimens were frozen in hexane cooled with dry ice. The frozen samples were

immersed in 5% carboxymethyl cellulose (CMC) gel for ten minutes and completely frozen with the CMC gel in cooled hexane. Next, the frozen blocks were fastened to the cryomicrotome (CM 1850; Leica Instruments, Germany) in the cryochamber (−22°C) and trimmed with a disposable tungsten carbide blade (Jung TC-65A, 35° angle; Leica Instruments). The trimmed surface was covered with a Cryofilm (FINETEC, Japan) using a brush to remove air bubbles behind the film. The sample was then cut at 5 to 7 μm thickness and dried at room temperature. Afterwards, the film was soaked briefly in ethanol and mounted on a glass slide so that the sampling side faced upward. Alizarin red/ alcian blue and Von Kossa/ van Gieson stainings were performed as before [16]. Stained slides were used for quantification of osteoid volume using the Bioquant Osteo software (Bioquant Osteoanalysis Co., Nashville, TN, USA).

Micro-computed tomography (μCT) analysis was carried out using Skyscan 1076 (Kontich, Belgium). Hind limbs were wrapped in tissue paper that was moistened with phosphate buffered saline (PBS) and scanned at 9 μm voxel size, applying an electrical potential of 50 kVp and current of 200uA, and using a 0.5mm aluminum filter. Skyscan software, Dataviewer, CTAn (Kontich, Belgium) was used to determine bone histomorphometric parameters. Cortical bone analysis was performed on the femoral and tibial diaphysis. As appropriate for skeletally-mature animals [26], each femur and tibia was analyzed with attention to limb length. For each limb, three regions were analyzed along the length of the limbs for cortical bone analysis. The regions, 747 μm along the femur and 711 μm along the tibia, were located at 14.3-28.6%, 42.9-57.1% and 71.4-85.7% of the distance between the growth plate and the throchanteric fossa for the femur and the growth plate to the distal junction of the tibia and fibula bone in the tibia. Cortical bone selection was done by contouring the periosteal tissue and excluding the marrow cavity. A global threshold was used to identify cortical bone and an erosion of one pixel was performed to eliminate partial volume effects and calculate the following parameters: cross-sectional tissue area (T.Ar), cross-sectional cortical bone area (B.Ar), cortical bone area fraction (B.Ar/T.Ar), cross-sectional bone thickness (Cs.Th) and tissue mineral density (TMD). TMD was calibrated against 2mm diameter hydroxyapatite (HA) phantoms appropriate for mouse samples. Additionally, a beam hardening correction algorithm was applied prior image reconstruction.

PP_i Assay

PP_i concentrations were determined by differential adsorption on activated charcoal of UDP-D-[6-^{3}H]glucose (Amersham Pharmacia) from the reaction product 6-phospho [6-^{3}H]gluconate, as described [27].

Statistical analyses

All numerical values are presented as mean values ± standard deviation (SD) unless mentioned otherwise. Non-parametric analysis was preferred for all parameters because of the small sample sizes. The Log-Rank test was used to compare survival curves. Fisher's exact test was used to compare the distribution of normal and abnormal radiographs between treatments. An Anova model was used to compare the average body weights between groups at each day, and the average bone lengths at the end of the study. For urine PP_i, bone osteoid and bone μCT measurements, the results are expressed as mean ± SEM, and data were analyzed using student's t test. P values less than 0.05 are considered significant.

Dose-Response Analysis

The conceptual pharmacodynamic (PD) models used to fit dose-response data are shown in Table 1. Akaike Information (AIC) and Schwarz Bayesian (SBC) criterion were used as a measure of goodness-of-fit to select the best model for each data set. When comparing

several models for a given data set, the model associated with the smallest AIC and SBC was selected during the model discrimination process. The correlation coefficient (r^2) and visual assessments of fit (VAF), absolute residual distribution, and coefficient of variation of PD parameters were also used for the model discrimination. Once the appropriate model was selected, the fit was re-run using predefined residual error models (additive, Poisson or proportional). The same criteria used to choose the model were applied to select the appropriate error model for each data set. PD analysis was performed using WinNonlin® Enterprise Edition software v5.2 (Pharsight Corporation, Mountain View, CA). All analyses were performed using full precision. Whenever possible, results were reported to 3 significant figures. PD parameters and their 95% confidence intervals were determined using WinNonlin 5.2.

Results

Changes in Survival

Survival of mice representing each treatment group was significantly improved when compared to Vehicle ($p<0.0001$) (Fig. 1). Differences were also statistically significant when the survival curves of the treated groups were compared ($p<0.0001$). Median survival was 19, 24, and 31 days in the Vehicle, Tx-0.5, and Tx-2.0 groups, respectively. Only one of 19 mice in Tx-8.2 died before the study was completed at age 43 days; thus, median survival could not be calculated for this group. However, there was a clear relationship between ENB-0040 daily dose and survival of the *Akp2*$^{-/-}$ mice.

Changes in body weight and femur/tibial length

Figure 2A depicts the growth curves of the mice. At the beginning of treatment, average daily body weights (BWs) showed no statistical difference between the newborn *Akp2*$^{-/-}$ mice of each treatment group and newborn WT mice. However, average BWs with Vehicle and Tx-0.5 were statistically lower compared to WT mice starting on Day 7 (4.156 g, 4.220 g and 4.726 g, respectively; $p=0.0068$ for Vehicle compared to WT, and $p=0.0216$ for Tx-0.5 compared to WT). For the Tx-2.0 group, BWs became statistically lower than WT starting on Day 16 (7.373 g and 8.248 g, respectively; $p=0.0496$). However, the average BWs for Tx-8.2 were never statistically different compared to WT mice. The Tx-2.0 and Tx-8.2 dose groups improved BWs compared to Vehicle-treated mice from Day 8 onwards, showing statistically significant differences (5.065 g for Tx-2.0 and 4.527 for Vehicle, $p=0.0446$; 5.065 g for Tx-8.2 and 4.527 for Vehicle, $p=0.0471$). Similarly, Tx-0.5 average BWs improved compared to Vehicle after Day 18 (6.532 g for Tx-0.5 and 5.456 g for Vehicle, $p<0.0001$). There was a clear relationship between ENB-0040 daily dose and preservation of healthy BW.

At study end, the average length of the femur in Tx-2.0 (11.92 ± 0.97 mm) and in Tx-8.2 (12.53 ± 0.77 mm) was shorter compared to the WT mice (13.35 ± 0.52 mm) ($p= 0.0010$ and $p=0.0021$, respectively) (Fig. 2B). However, the average length of the femur in Tx-2.0 was not statistically different compared to Tx-8.2 ($p=0.1277$). The average length of the tibia in Tx-2.0 (15.39 ± 0.64 mm) and Tx-8.2 (15.70 ± 0.87 mm) was shorter compared to WT mice (16.61 ± 0.49 mm) ($p= 0.0046$ and $p=0.0009$, respectively). The average length of the tibia in Tx-2.0 was not statistically different compared to Tx-8.2 ($p=0.4368$). There was a trend towards preservation of bone length in *Akp2*$^{-/-}$ mice with increasing doses of ENB-0040. Deaths of the Vehicle or Tx-0.5 mice precluded age-matched bone length analysis.

Improved skeletal phenotype in Akp2$^{-/-}$ mice receiving ENB-0040 treatment

The radiographs of untreated *Akp2*$^{-/-}$ mice (Vehicle) showed profound skeletal abnormalities such as bowed and fractured femora and tibiae, reduced tissue mineral density

(TMD) in femora, tibiae, incisors and molars, shorter vertebrae, and increased spaces between adjacent vertebrae. All these abnormalities showed slight improvement with the lowest dose of ENB-0040 (Tx-0.5 group), and considerable improvement within the Tx-2.0 group. There was callus formation at the sites of fractures in femur and tibia, improved bone morphology, increased TMD, and reduced intervertebral spaces in the treated mice (Fig. 3). μCT analysis of the long bones from 22 day-old untreated *Akp2*$^{-/-}$ mice (Vehicle) and treated (Tx-0.5 and Tx-2.0) mice showed a clear and significant improvement in the bone morphology and TMD proportional to the treatment administered (Fig. 4; Table 2). The *Akp2*$^{-/-}$ mice femora showed ~60% less mineral density than the WT mice. Low dose (Tx-0.5) treatment improved the TMD to ~70%, and a higher dose (Tx-2.0) improved it to ~80% of the WT values (vehicle versus Tx-2.0, p=0.02, significant) and in tibiae the Tx-2.0 group showed ~93% (vehicle Vs Tx-2.0, p= 0.007, significant; Tx-2.0 versus WT, p = 0.2, not significant) recovery of TMD. Morphologically, the *Akp2*$^{-/-}$ bones had only 23% cortical thickness in the tibiae compared to WT mice. However, in the Tx-2.0 treatment group, cortical thickness seemed improved to 62% of WT (Tx-2.0 Vs WT, p = 0.084, but non-significant) (Table 2).

Histological analysis of 44-day-old treated tibiae stained with alizarin red/alcian blue (Fig. 5A) showed increased mineralization of the trabecular bone in the TX-8.2 group. Von Kossa/Van Gieson staining (Fig. 5B) also revealed decreased amounts of unmineralized osteoid in the Tx-8.2 group, which showed no statistically significant difference when compared to the WT mice. The OV/BV % values obtained were as follows: Tx-2.0= 5.723 ± 2.036 (N= 3); Tx-8.2= 0.013 ± 0.004 (N= 3); WT= 0.009 ± 0.0005 (N= 3); Tx-8.2 group showed a non-significant difference when compared to WT, p= 0.26. Of interest, urinary PP_i concentrations remained high in all treatment groups, despite the correction of plasma PP_i levels and the obvious improvement of the skeletal condition in the treated mice (Fig. 6).

The radiographic results for each treatment group, i.e., *Akp2*$^{-/-}$ receiving vehicle alone versus 0.5, 2.0, or 8.2 mg/kg/day ENB-0040, are summarized in Table 3. Here, the distribution between normal and abnormal radiographic images are presented, with the percentages given in parentheses. At necropsy, 10%, 15%, and 25% of mice receiving Vehicle had normal left foot, rib cage, or lower limb radiographs, respectively, compared to 100% normal appearance for the WT mouse specimens (data not shown). However, the percentage of animals with normal mineralization of the left foot was improved from 10% with Vehicle to 39, 85, and 100% with increasing doses of ENB-0040. The efficacy of the 2.0 and 8.2 mg/kg doses was statistically significant when compared to Vehicle ($p<0.0001$), whereas the smallest (0.5 mg/kg) dose only approached statistical significance (p=0.0577). Inter-treatment comparisons showed that Tx-2.0 and Tx-8.2 were more effective compared to Tx-0.5 (p=0.0063 and $p<0.0001$, respectively). However, Tx-8.2 efficacy was not better when compared to Tx-2.0 (p=0.2308).

Similarly, radiographic analysis of the rib cage and lower limbs showed the distribution presented in Table 3. For the rib cage endpoint, the percentage of animals with normal bony structures was increased from 15% with Vehicle to 39, 80, and 88% with increasing doses of ENB-0040. The efficacies of the 2.0 and 8.2 mg/kg doses were statistically significant when compared to Vehicle ($p<0.0001$), whereas the 0.5 mg/kg level was not (p=0.1440). Inter-treatment comparisons showed that Tx-2.0 and Tx-8.2 were more effective compared to Tx-0.5 (p=0.0189 and p=0.0045, respectively). The efficacy of Tx-8.2 was not different from Tx-2.0 (p=0.6665). The percentage of mice with normal bony structures of the lower limbs increased from 25% with Vehicle to 56, 80, and 84% with increasing doses of ENB-0040 (Table 3). The efficacy of the 2.0 and 8.2 mg/kg dose was statistically significant when compared to Vehicle (p=0.0012 and $p<0.0001$, respectively), whereas 0.5 mg/kg only approached statistical significance (p=0.0960). Inter-treatment comparisons showed that

Tx-2.0 was not more effective compared to Tx-0.5 (p=0.1643), but 8.2 mg/kg approached statistical significance (p=0.0789). The efficacy of Tx-8.2 was not different from Tx-2.0 (p>0.9999).

We examined the dose response to ENB-0040 treatment by evaluating the effect of various doses on the radiographic image distribution (RID) pharmacodynamic endpoint. According to Akaike Information (AIC) and Schwarz Bayesian Criterion (SBC) values, the Simple E_{max} Model with Baseline fitted the Dose vs. RID relationship adequately. Visual assessments of fit and absolute residual distributions indicated that the Simple E_{max} with E_0 Model and a proportional error appeared to be the best weighting scheme for the Dose-RID relationship. We found a clear relationship between daily dose of ENB-0040 and percent of mice with normal bony structures of the foot, rib cage, and lower limbs. The 80% effective dose (ED_{80}) was estimated to be 3.2 mg/kg/day for feet, 2.8 mg/kg/day for rib cage, and 2.9 mg/kg/day for lower limbs (Fig. 7). The overall pharmacokinetics/PD relationship was characterized by a steep increase in the range 0 - 5 mg/kg/day, with maximum effect (~100%) observed at 6 to 8 mg/kg/day.

Discussion

In 2008, we established that EzRT using daily SC injections of bone-targeted, recombinant, human TNSALP, i.e., sALP-FcD_{10} (ENB-0040), prevented infantile HPP in the *Akp2*$^{-/-}$ mouse model [23]. We evaluated survival, growth rates, serum levels of sALP-FcD_{10} activity, calcium, PP_i, and PLP, as well as skeletal and dental manifestations of HPP by radiography, μCT, and histomorphometry. *Akp2*$^{-/-}$ mice receiving high-doses (8.2 mg/kg/day) of sALP-FcD_{10} for 8 weeks grew normally and appeared well without skeletal disease or epilepsy [23]. More recently, we demonstrated that treatment with high-dose (8.2 mg/kg/day) of sALP-FcD_{10} prevented hypomineralization of alveolar bone, dentin, and cementum as assessed by micro-computed tomography and histology [24].

The objective of the present study was to define the dose response relationship between increasing amounts of cGMP-produced ENB-0040 using bolus SC injections and the therapeutic response after 43 days in anticipation of clinical trials. Endpoints were survival, body weight, bone length of the tibiae and femora, and bone mineralization defects assessed using radiographs of the feet, rib cage, and lower limbs. To-date, these parameters have represented good indicators of correction of the HPP phenotype in this animal model. Also, the radiographic manifestations of HPP are readily observed in affected infants and, thus, are an important endpoint in preclinical proof-of-concept studies for extrapolation from mice to humans [2, 3]. In addition, we used μCT and histomorphometric analysis to document the improvement in *Akp2*$^{-/-}$ bone mineralization status for representative age groups undergoing treatment.

We documented a clear relationship between daily dose of ENB-0040 and the percent of mice with normal bony structures of the foot, rib cage, and lower limbs. We focused on establishing the effective dose in 80% of the mice (ED_{80}). The 80% effective dose in mice was ~ 3.2 mg/kg/day for feet, ~ 2.8 mg/kg/day for rib cage, and ~ 2.9 mg/kg/day for lower limbs. These ED_{80} doses are consistent with our previous experience showing a better skeleton in a short-term, 15-day treatment of *Akp2*$^{-/-}$ animals using 2 mg/kg/day of ENB-0040 [23].

Of interest, in this new study, we found that, despite the correction of plasma PP_i levels by ENB-0040 treatment already documented [23], urinary PP_i concentrations remained elevated for all treatment groups. This is important because measurement of urinary PP_i is used as a diagnostic marker for HPP [2, 3]. We interprete this result to indicate that urinary

PP_i reflects local production or degradation of PP_i in the kidney. Since ENB-0040 is a bone-targeted form of TNSALP, ENB-0040 would not accumulate in the kidneys to contribute to renal PP_i metabolism. Thus, urinary PP_i might not be a good marker to evaluate ENB-0040 treatment for HPP patients. Instead, radiographic changes remain the best mechanism to monitor improvement of the HPP skeleton when there is rickets [23].

Our studies using ENB-0040, produced under cGMP conditions, confirm and extend our previous data regarding the prevention of HPP in *Akp2*$^{-/-}$ mice by administration of this bone-targeted form of TNSALP from birth [23], and helped to set the stage for the clinical trials now underway for patients with HPP (http://clinicaltrials.gov/). The ED_{80} documented in this study, along with enzyme concentrations measured during the animal efficacy studies and ENB-0040 pharmacokinetic data, were used to estimate the minimum effective concentrations for *Akp2*$^{-/-}$ mice. Initial dosing of ENB-0040 for clinical trials was then based on: 1) dose-response data reported here using the *Akp2*$^{-/-}$ mouse model of infantile HPP, 2) efficacy observed in treated *Akp2*$^{-/-}$ mice that achieved serum ALP activity in the range of 650 – 1000 U/L; 3) the No-Observed-Adverse-Effect Level (NOAEL) in the more sensitive species (rats and monkeys) established in one-month intravenous (IV) toxicology studies and one-month IV/subcutaneous (SC) bridging and tolerability study in rats; 4) a safety factor of 10 applied to the NOAEL; and 5) results from a multicenter, open-label, dose-escalating study of the safety, tolerability, and pharmacology of ENB-0040 in six adults with HPP who received one dose of 3 mg/kg IV, and then either 1 or 2 mg/kg ENB-0040 SC once weekly for three weeks.

Acknowledgments

This work was funded by Enobia Pharma, Inc and by grant DE12889 from the National Institutes of Health, USA. We acknowledge the expert technical contributions and dedication from Enobia employees, Nathalie Brissette, Marie-Ève Longchamps, Caroline Meilleur, Johanne Pion, Annie Salesse, Claire Vézina, Thomas Loisel, Julie Guimond, Geneviève Hélie, Éric Leblanc, Line Lespérance, and Jacqueline Yep.

References

[1]. Fraser D. Hypophosphatasia. Am J Med. 1957; 22:730–746. [PubMed: 13410963]

[2]. Whyte, MP. Hypophosphatasia. In: Scriver, CR.; Beaudet, AL.; Sly, WS.; Valle, D., editors. The Metabolic and Molecular Bases of Inherited Disease. 8th Edition. McGraw-Hill; New-York, N.Y. U.S.A.: 2001. p. 5313-5329.

[3]. Whyte, MP. Hypophosphatasia: Nature's Window On Alkaline Phosphatase Function In Humans. In: Bilezikian, JP.; Raisz, LG.; Martin, TJ., editors. Principles Of Bone Biology. 3rd Ed.. Academic Press; San Diego, California: 2008. p. 1573-1598.

[4]. Weiss MJ, Cole DE, Ray K, Whyte MP, Lafferty MA, Mulivor RA, Harris H. A missense mutation in the human liver/bone/kidney alkaline phosphatase gene causing a lethal form of hypophosphatasia. Proc Natl Acad Sci U S A. 1988; 85:7666–7669. [PubMed: 3174660]

[5]. Henthorn PS, Whyte MP. Missense mutations of the tissue-nonspecific alkaline phosphatase gene in hypophosphatasia. Clin Chem. 1992; 38:2501–2505. [PubMed: 1360878]

[6]. Henthorn PS, Raducha M, Fedde KN, Lafferty MA, Whyte MP. Different missense mutations at the tissue-nonspecific alkaline phosphatase gene locus in autosomal recessively inherited forms of mild and severe hypophosphatasia. Proc Natl Acad Sci U S A. 1992; 89:9924–9928. [PubMed: 1409720]

[7]. Fallon MD, Teitelbaum SL, Weinstein RS, Goldfischer S, Brown DM, Whyte MP. Hypophosphatasia: clinicopathologic comparison of the infantile, childhood, and adult forms. Medicine. 1984; 63:12–24. [PubMed: 6690884]

[8]. Narisawa S, Fröhlander N, Millán JL. Inactivation of two mouse alkaline phosphatase genes and establishment of a model of infantile hypophosphatasia. Dev Dyn. 1997; 208:432–446. [PubMed: 9056646]

[9]. Fedde KN, Blair L, Silverstein J, Coburn SP, Ryan LM, Weinstein RS, Waymire K, Narisawa S, Millán JL, MacGregor GR, Whyte MP. Alkaline phosphatase knockout mice recapitulate the metabolic and skeletal defects of infantile hypophosphatasia. J Bone Miner Res. 1999; 14:2015–2026. [PubMed: 10620060]

[10]. Waymire KG, Mahuren JD, Jaje JM, Guilarte TR, Coburn SP, MacGregor GR. Mice lacking tissue non-specific alkaline phosphatase die from seizures due to defective metabolism of vitamin B-6. Nat Genet. 1995; 11:45–51. [PubMed: 7550313]

[11]. Baumgartner-Sigl S, Haberlandt E, Mumm S, Scholl-Bürgi S, Sergi C, Ryan L, Ericson KL, Whyte MP, Högler Wl. Pyridoxine-responsive seizures as the first symptom of infantile hypophosphatasia caused by two novel missense mutations (c.677T>C, p.M226T; c.1112C>T, p.T371I) of the tissue-nonspecific alkaline phosphatase gene. Bone. 2007; 40:1655–1661. [PubMed: 17395561]

[12]. Narisawa S, Wennberg C, Millán JL. Abnormal vitamin B6 metabolism in alkaline phosphatase knock-out mice causes multiple abnormalities, but not the impaired bone mineralization. J Pathol. 2001; 193:125–133. [PubMed: 11169525]

[13]. Meyer JL. Can biological calcification occur in the presence of pyrophosphate? Arch Biochem Biophys. 1984; 231:1–8. [PubMed: 6326671]

[14]. Hessle L, Johnson KA, Anderson HC, Narisawa S, Sali A, Goding JW, Terkeltaub R, Millán JL. Tissue-nonspecific alkaline phosphatase and plasma cell membrane glycoprotein-1 are central antagonistic regulators of bone mineralization. Proc Natl Acad Sci U S A. 2002; 99:9445–9449. [PubMed: 12082181]

[15]. Harmey D, Hessle L, Narisawa S, Johnson KA, Terkeltaub R, Millán JL. Concerted regulation of inorganic pyrophosphate and osteopontin by *Akp2*, *Enpp1* and *Ank*. An integrated model of the pathogenesis of mineralization disorders. Am J Pathol. 2004; 164:1199–1209. [PubMed: 15039209]

[16]. Murshed M, Harmey D, Millán JL, McKee MD, Karsenty G. Broadly expressed genes accounts for the special restriction of ECM mineralization to bone. Genes Dev. 2005; 19:1093–1104. [PubMed: 15833911]

[17]. Harmey D, Johnson KA, Zelken J, Camacho NP, Hoylaerts MF, Noda M, Terkeltaub R, Millán JL. Elevated osteopontin levels contribute to the hypophosphatasia phenotype in *Akp2*$^{-/-}$ mice. J Bone Miner Res. 2006; 21:1377–1386. [PubMed: 16939396]

[18]. Millán, JL. Mammalian alkaline phosphatases. From biology to applications in medicine and biotechnology. Wiley-VCH Verlag GmbH & Co; Weinheim, Germany: 2006. p. 1-322.pgs

[19]. Whyte MP, Valdes R Jr, Ryan LM, McAlister WH. Infantile hypophosphatasia: Enzyme replacement therapy by intravenous infusion of alkaline phosphatase-rich plasma from patients with Paget bone disease. J Pediatr. 1982; 101:379–386. [PubMed: 7108657]

[20]. Whyte MP, McAlister WH, Patton LS, Magill HL, Fallon MD, Lorentz WB Jr, Herrod HG. Enzyme replacement therapy for infantile hypophosphatasia attempted by intravenous infusions of alkaline phosphatase-rich Paget plasma: Results in three additional patients. J Pediatr. 1984; 105:926–933. [PubMed: 6502342]

[21]. Weninger M, Stinson RA, Plenk H Jr, Böck P, Pollak A. Biochemical and morphological effects of human hepatic alkaline phosphatase in a neonate with hypophosphatasia. Acta Paediatr Scand Suppl. 1989; 360:154–160. [PubMed: 2642253]

[22]. Whyte MP, Habib D, Coburn SP, Tecklenburg F, Ryan L, Fedde KN, Stinson RA. Failure of hyperphosphatasemia by intravenous infusion of purified placental alkaline phosphatase (ALP) to correct severe hypophosphatasia: Evidence against a role for circulating ALP in skeletal mineralization. J Bone Miner Res. 1992; 7(Suppl 1):S155.

[23]. Millán JL, Narisawa S, Lemire I, Loisel TP, Boileau G, Leonard P, Gramatikova S, Terkeltaub R, Pleshko Camacho N, McKee MD, Crine P, Whyte MP. Enzyme replacement therapy for murine hypophosphatasia. J Bone Miner Res. 2008; 23:777–787. [PubMed: 18086009]

[24]. McKee MD, Nakano Y, Masica DL, Gray JJ, Lemire I, Heft R, Whyte MP, Crine P, Millán JL. Enzyme replacement prevents dental defects in a mouse model of hypophosphatasia. J. Dental Res. 2011 In Press.

[25]. Kawamoto T. Use of a new adhesive film for the preparation of multi-purpose fresh-frozen sections from hard tissues, whole-animals, insects and plants. Arch. Histol. Cytol. 2003; 66:123–143. [PubMed: 12846553]

[26]. Bouxsein ML, Boyd SK, Christiansen BA, Guldberg RE, Jepsen KJ, Muller R. Guidelines for assessment of bone microstructure in rodents using micro-computed tomography. J Bone Miner Res. 2010; 25:1468–1486. [PubMed: 20533309]

[27]. Johnson K, Vaingankar S, Chen Y, Moffa A, Goldring M, Sano K, Jin-Hua P, Sali A, Goding J, Terkeltaub R. Differential mechanisms of inorganic pyrophosphate production by plasma cell membrane glycoprotein-1 and B10 in chondrocytes. Arthritis Rheum. 1999; 42:1986–1997. [PubMed: 10513816]

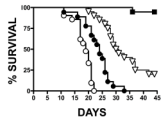

Fig. 1.

Percentage survival of *Akp2*$^{-/-}$ mice receiving either Vehicle (◯) or escalating doses of ENB-0040, i.e. Tx-0.5 (●), Tx-2.0 (▽), or Tx-8.2 (■).

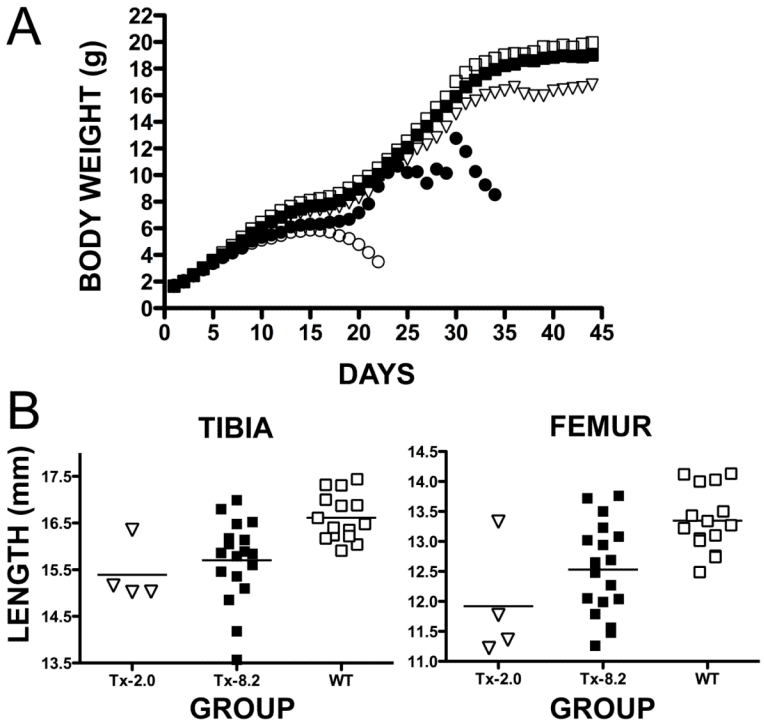

Fig. 2.

Changes in body weight with age and tibiae/femora lengths as a function of treatment dose. Panel A shows average daily body weights of *Akp2*$^{-/-}$ mice, from Day 1 to the end of the study, treated with Vehicle (◯), Tx-0.5 (●), Tx-2.0 (▽), Tx-8.2 (■) or untreated WT mice (□). Panel B shows individual lengths of the left tibiae and femora at the end of the study for the Tx-2.0 (▽) and Tx-8.2 (■) treatment groups compared to WT mice (□).

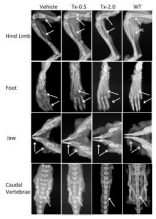

Fig 3.

Representative radiographs of hind limb, foot, jaw bones and caudal vertebrae specimens from 22-day-old *Akp2*$^{-/-}$ mice treated with vehicle, Tx-0.5, Tx-2.0, and untreated WT mice (radiographic magnification 5X). Arrows indicate improvement in the mineralization of tibia, femur, metatarsals, finger bones, incisors and molars, fracture healing in the tibia and femur, and reduced spaces between adjacent vertebrae of spine in the treated mice compared to the untreated mice.

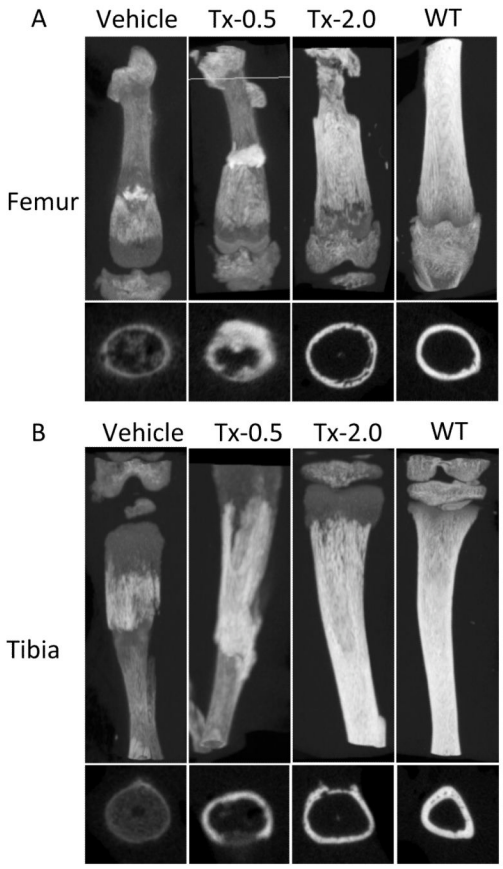

Fig 4.

μCT images of (A) Femora and (B) Tibiae of the 22-day-old *Akp2*$^{-/-}$ mice treated with vehicle, Tx-0.5, Tx-2.0, and untreated WT mice. The images clearly show improved TMD and callus formation at the site of fractures in the treated mice. Transaxial views at the bottom.

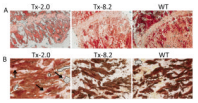

Fig 5.

Histological analysis of tibiae and femora from 44-day-old Tx-2, Tx-8.2, and untreated WT mice. (A) Alizarin red/ alcian blue staining of the tibia revealed increased bone mineralization with increased dosage (Tx-8.2) of ENB-0040, which is comparable to the WT mice. (B) Von kossa/Van Gieson staining of the femoral section also shows reduction in osteoid volume with increased dosage (Tx-8.2) of ENB-0040. Arrows indicate the presence of osteoid in Tx-2.0 group which was significantly reduced in the Tx-8.2 group and showed no significant difference from WT mice (Tx-2.0: OV/BV= 5.723%, Tx-8.2: OV/BV= 0.013%, WT: OV/BV= 0.009%. TX-8.2 versus WT: non-significant, p= 0.26).

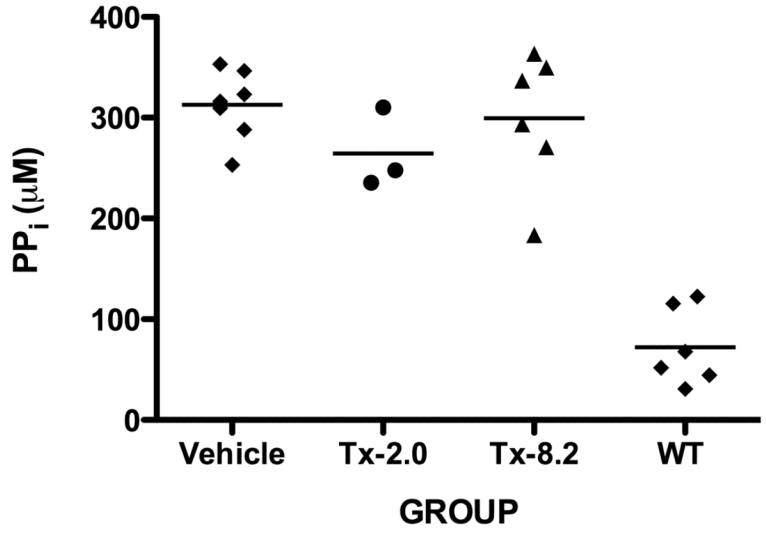

Fig. 6.

PP_i concentrations in the urine of *Akp2*$^{-/-}$ mice receiving vehicle or escalating doses of ENB-0040, i.e. Tx-2.0, Tx-8.2, and WT. No significant reduction in the urine PP_i levels was observed for the treated compared to untreated mice.

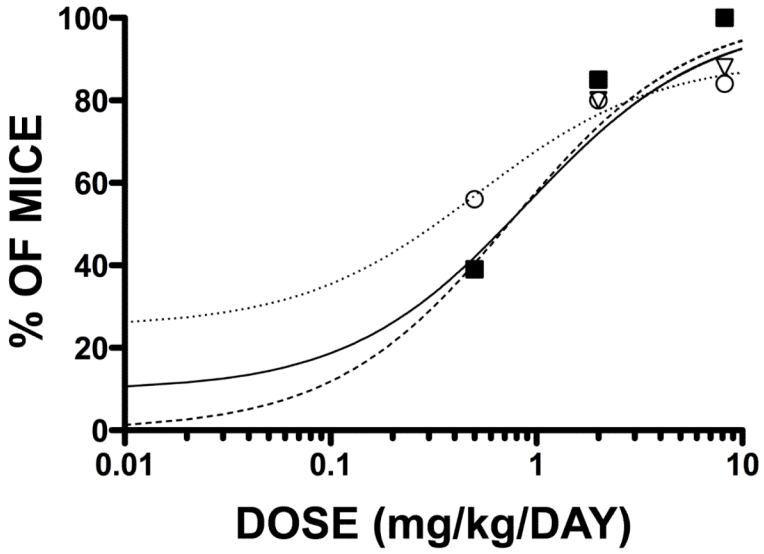

Fig. 7.

Percentage of *Akp2*$^{-/-}$ mice considered normal as a function of ENB-0040 dose for feet (□), rib cage (▼), and lower limbs (◯).

Table 1

Conceptual Pharmacodynamic (PD) Models

Model	Equations
Linear Model	$E= E_0 + S * C$
Simple E_{max} Model	$E= (E_{max} * C)/(C+ED_{50})$
Simple E_{max} Model with E_0	$E=E_0+ (E_{max}-E_0)* (C/(C+ED_{50}))$
Sigmoid E_{max} Model	$E=(E_{max} * C^{\gamma})/(C^{\gamma} +ED_{50}^{\gamma})$
Sigmoid E_{max} Model with E_0	$E=E_0 + (E_{max} -E0)*(C^{\gamma} /(C^{\gamma} + ED_{50}^{\gamma}))$
Weibull	$E = E_{max} * (1-\exp(-(C/ ED_{50})^S))$
Makoid-Banakar	$E = E_{max} *(C/Cmax)^S*\exp(S*(1-C/Cmax))$, when $C \leq Cmax$, $E = E_{max}$, when $C > C_{max}$

E= effects, C= Dose, S= Slope, γ= sigmoidicity factor, C_{max} = maximal dose, E_{max}= maximal effects, E_0= baseline effects at C=0, ED_{50}= dose that induced 50% of E_{max}

Table 2

μCT analysis of the cortical bones in femora and of tibiae from 22-day-old *Akp2*$^{-/-}$ mice treated with vehicle, Tx-0.5, Tx-2.0, and untreated WT mice. The following parameters were measured: mean total cross-sectional tissue area (T.Ar), mean total cross-sectional bone area (B.Ar), percent bone area (B.Ar/T.Ar), cross-sectional thickness (Cs. Th), and Tissue mineral density (TMD)

	T.Ar (mm^3)	B.Ar mm^3)	B.Ar/T.Ar (%)	Cs.Th mm	TMD g/cm^3	SEM
FEMUR						
Vehicle	0.427	0.119	24.11	0.038	0.578	0.024
Tx-0.5	0.606	0.252	37.55	0.092	0.665	0.095
Tx-2.0	0.715	0.249	33.32	0.061	0.740	0.049
WT	1.781	1.703	58.19	0.124	0.951	0.057
TIBIA						
Vehicle	0.297	0.062	18.40	0.031	0.586	0.040
Tx-0.5	0.517	0.137	30.60	0.072	0.685	0.034
Tx-2.0	0.576	0.254	46.10	0.082	0.871	0.059
WT	0.705	0.420	60.18	0.132	0.936	0.041

Bone. Author manuscript; available in PMC 2012 August 1.

Table 3

Distribution of radiographs of the feet, rib cage, and lower limbs of *Akp2*$^{-/-}$ mice receiving vehicle or 0.5, 2.0, or 8.2 mg/kg/day ENB-0040, displaying normal bony structures

	Number of mice with normal bony structures (%)		
Group	**Left Foot**	**Rib Cage**	**Right Lower Limb**
Vehicle (N=20)	2 (10)	3 (15)	5 (25)
Tx-0.5 (N=18)	7 (39)	7 (39)	10 (56)
Tx-2.0 (N=20)	17 (85)	16 (80)	16 (80)
Tx-8.2 (N=19) *	19 (100)	15 (88)	16 (84)

* N=17 for rib cage specimens